1 # System vulnerability and risk assessment of railway systems to flood events

2 ## based on national and river basin scale in China

3 Weihua Zhu[1,2], Kai Liu [1, 2*], Ming Wang [1,2], Philip J. Ward[3], Elco E. Koks[3]

4 *[1] School of National Security and Emergency Management, Beijing Normal University,*

5 *Beijing 100875, China*

6 *[2] Academy of Disaster Reduction and Emergency Management, Beijing Normal*

7 *University, Beijing 100875, China*

8 *[3]Institute for Environmental Studies (IVM), Vrije Universiteit Amsterdam, 1081 HV*

9 *Amsterdam, Netherlands*

10 Correspondence to Kai Liu (liukai@bnu.edu.cn).

12 **ABSTRACT:** Floods have negative effects on the reliable operation of transportation

13 systems. In China alone, floods cause an average of ~1125 hours of railway service

14 disruptions per year. In this study, we present a simulation framework to analyse the

15 system vulnerability and risk of the railway system to floods. To do so, first, we

16 developed a novel methodology for generating flood events at both the national and

17 river basin scale. Based on flood hazard maps of different return periods, independent

18 flood events are generated using the Monte Carlo sampling method. Combined with

19 network theory and spatial analysis methods, the resulting event set provides the basis

20 for national- and provincial-level railway risk assessments, focusing in particular on train

21 performance loss. Applying this framework to the Chinese railway system, we show that

the system vulnerability of the Chinese railway system to floods in different basins is highly heterogeneous as a result of spatial variations in the railway topology and traffic flows. Flood events in the Yangtze River Basin show the largest impact on the national railway system, with approximately 40% of the national daily trains being affected by a 100-year flood event in that basin. At the national level, the average number of daily affected trains and passengers for the national system are approximately 200 trips and 165,000 people (2.7% and 2.8% of the total daily numbers of trips and passengers), respectively. The event-based approach presented in this study shows how we can identify critical hotspots within a complex network, taking the first steps in developing climate-resilient infrastructure.

KEYWORDS: river basin flooding; railway system; risk assessment; system vulnerability

1. Introduction

Floods can have negative effects on transportation systems through both the destruction of physical infrastructure and the disruption of freight and traffic flows (Reed, 2004; Moran et al., 2010; Benn, 2013; Kellermann et al., 2015). For example, during the Tbilisi (Georgia) floods in June 2015, the estimated damage in terms of replacing affected assets was 14.8 million USD, whilst losses related to increases in travel time and higher operating costs were estimated at approximately three million USD (up until autumn 2015) (GFDRR, 2015). In May and June 2013, the Austrian Federal Railways faced severe damage by the major floods in central Europe, with a total cost

of more than 84 million USD. The event caused extensive damage to track structures

and also caused widespread service disruptions, despite many protective actions that

had been adopted ahead of time (Kellermann et al., 2016). In China, over 2146 rail

service disruption events and over 20,825 hours of discontinued service due to flooding

were reported from 2000 to 2016 (Editorial Board of China Railway Yearbook, 2001-

2017). In 2016, the direct economic loss of the Chinese railway system caused by floods

was approximately 80 million USD (Editorial Board of China Railway Yearbook, 2001-

2017). As such, there is a clear need to evaluate the vulnerability of the transportation

system to extreme flood hazards and to identify high-risk transportation components

to make the transportation systems safer and more effective for operation and

maintenance.

Many studies have investigated flood impacts on transportation systems, focusing on

either flood vulnerability of assets (Kellermann et al., 2015; Pregnolato et al., 2017;

Singh et al., 2018; Koks et al., 2019) or the risk to the entire system (Gil and Steinbach,

2008; Kellermann et al., 2016; Lamb et al., 2019). In these studies, flood vulnerability is

usually defined as the relationship between the characteristics of the transportation

components (i.e., the physical structure, traffic flow and traffic velocity) and the

variables characterizing the intensity of the flood hazard (i.e., flood depth and flood

velocity) (Pregnolato et al., 2017). However, as major river floods are usually driven by

large-scale atmospheric circulations (Prudhomme and Genevier, 2011; Lavers et al.,

2013) and affect large areas, they can disrupt several components concurrently across

1 a network system (Becker and Grünewald, 2003; Kundzewicz et al., 2013). Within a

2 network system, the impact on operational performance is often the result of failure of

3 multiple components in the aftermath of an event (Gong et al., 2017). As such, a

4 system-level perspective is essential to properly assess transportation system

5 vulnerability due to flooding.

6   Some studies have assessed transportation vulnerability to natural hazards from a

7 system-level perspective (Chang et al., 2010; Hong et al., 2015). Chang et al. (2010)

8 investigated the potential impacts of climate change on travel disruption in the

9 metropolitan area of Portland, Oregon. They combined a hydrologic, hydraulic model

10 and a travel forecast model to process their study. Hong et al. (2015) assessed the

11 Chinese railway system's vulnerability in terms of traffic flow loss based on historical

12 flood events from 1981 to 2010. Unfortunately, due to the widespread lack of

13 appropriate historical flood hazard data and computational issues with running large-

14 scale hydraulic models (Sene 2008; Chang et al. 2010), research so far has been carried

15 out only on a case-study basis where historical scenarios are available (Hong et al.,

16 2015). However, for inter-city and inter-country trade, national and global-scale

17 transportation systems have flourished in recent decades. Examples include Pan-

18 European transportation corridors (Janic and Vleugel, 2012) and the railway system of

19 the Belt and Road Initiative (Yang et al. 2018); therefore, large-scale flood event data

20 and methods should be improved to assess system-level vulnerability and risk on

21 operational performance for such large spatial transportation systems.

1   The recent development of global flood hazard maps (Alfieri et al., 2013; Hirabayashi

2   et al., 2013; Ward et al., 2013; Sampson et al., 2015; Dottori et al., 2016) has paved the

3   way for performing large-scale flood risk assessments. These global flood hazard maps

4   have been widely applied to assess the global risk to flooding in terms of population

5   (Ward et al. 2013; Arnell et al. 2016; Dottori et al. 2016), gross domestic product (GDP)

6   (Ward et al., 2013; Winsemius et al., 2013), economic damage (Ward et al., 2013;

7   Dottori et al., 2016; Winsemius et al., 2016; Ward et al., 2017), and transportation

8   infrastructure (Koks et al., 2019). Koks et al. (2019), for example, assessed the direct

9   economic damage to transportation infrastructure assets using a conventional damage

10   assessment approach through asset-specific fragility curves based on global flood data.

11   Studies such as these facilitate a better understanding of the impacts of flood hazards

12   on large-scale transportation systems and provide up-to-date knowledge on risk

13   analysis frameworks.

14   This study aims to develop a framework to quantify the system vulnerability and risk

15   to transportation systems in terms of operational performance loss under large-scale

16   flood hazards. System vulnerability in this study is represented as the system

17   performance loss with different flood intensities. When assessing possible cascading

18   effects, the use of independent flood events is necessary (Nones and Pescaroli, 2016),

19   as the presented floods in regional-or national-scale flood footprints, which show the

20   flood depth for a given return period in that area, may not all happen at the same time.

21   To overcome the shortcomings in existing studies, we develop a simplified practicable

1 and novel method for generating a set of independent flood events at the national and

2 river basin scale. The independent floods are generated using a curve fitting method

3 and Monte Carlo sampling method based on global flood hazard model maps and river

4 basins. By coupling simulated flood events with the railway network using the spatial

5 analysis method, we identify the railway failure hotspots caused by floods. At the same

6 time, the potential performance loss is assessed using network theory. We illustrate our

7 methodology by applying it to the Chinese railway system.

8   The remainder of the paper is organized as follows. In Section 2, we propose a

9 framework for the evaluation of system vulnerability and risk of flood hazards to

10 transportation systems and use the Chinese railway system for application, including

11 how to generate flood events, define the network system for the transportation system,

12 calculate system vulnerability metrics, and quantify flood risk. Section 3 presents the

13 main findings and results. Section 4 and Section 5 provide the discussion and conclusion,

14 respectively, to this article.

15 ## 2. Data and method

16   Flood risk can be defined as a function of flood hazard, exposure and its related

17 vulnerability. A flood hazard is usually characterised by its intensity and occurrence

18 probability; exposure refers to the population and assets exposed to flooding; and

19 vulnerability is often defined as the loss ratio of people or assets suffered to different

20 intensity of hazard (Gouldby and Samuels, 2009; Haimes, 2009; UNISDR, 2011;

Winsemius et al., 2013). In this work, exposure is represented by the railway network

exposed to the flood hazard. Asset vulnerability is defined as the failure of a railway

asset based on the design standard and is expressed as a failure threshold. If the failure

threshold is exceeded, the service of the component is assumed to be disrupted,

resulting in a 100% performance loss of that asset. System vulnerability is represented

as the system performance loss with different flood intensities. Risk is calculated as the

expected annual performance loss at the national and provincial levels.

Figure 1 presents an overview of the framework used in this study. First, we generate

a national- and river basin-scale flood event set. To do this, we use flood hazard maps

for different return periods at the national scale, taken from a global flood hazard model.

We then divide these into flood hazard maps for the major river basins and use a curve-

fitting method to estimate the flood depth for any return period for any cell. We then

apply a Monte Carlo sampling method (Metropolis 1987) to generate the flood events

per river basin and aggregate these events to the national scale. Second, we define the

railway system as a network using network theory (Newman, 2010). Third, we intersect

the flood events with the railway network to identify the disrupted segments in the

railway system based on a pre-defined failure threshold. In the last part of our analysis,

we assess the system vulnerability and risk in terms of several performance loss metrics,

including the daily cancelled trains and passengers influenced by cancelled train, the

daily detoured trains and passengers influenced by detoured train, the daily affected

trains and affected passengers, as well as the total increased time and the average

1 increased time for the detoured trains. We also analyse the parameters in the failure

2 threshold sensitivity to the risk result and the related risk uncertainty.
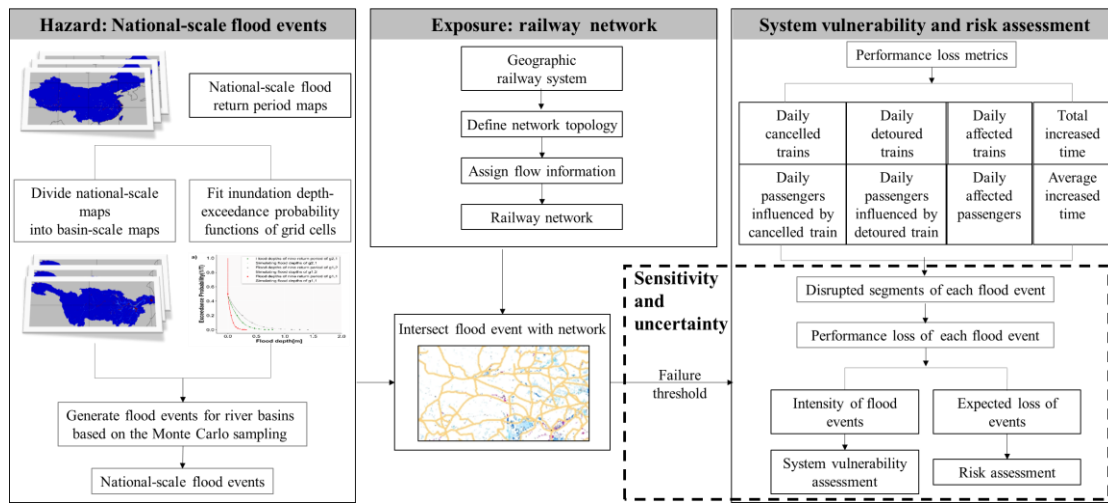
4 *Fig. 1 Methodology of the flood system vulnerability and risk assessment of railway*

5 *infrastructure. Railway geometries © OpenStreetMap contributors 2019. Distributed*

6 *under the Open Data Commons Open Database License (ODbL) v1.0.*

2.1 National-scale flood event generation

8 To ensure the estimation is as accurate as possible for an event-based flood risk

9 assessment, a large number of independent flood events are required (Speight et al.,

10 2017; Wu, 2019; Zhu et al., 2020). In this study, we apply a curve-fitting method and a

11 Monte Carlo sampling method to generate independent flood events using global flood

12 hazard maps from GLOFRIS for multiple return periods (Ward et al., 2013). In brief, for

13 each grid cell, we obtain the flood depth from the flood hazard maps for nine different

14 return periods (2-1000 years). We then fit an inundation depth-exceedance probability

15 function through these data points, which is used to estimate the flood depths for any

16 return period. Based on these functions per cell, we apply a Monte Carlo sampling

1   method to produce basin-specific flood events, which are further combined into a

2   national independent flood event set (see Section 2.1.3). In this study, we assume that

3   a flood event within one basin will produce a flood with the same intensity (return

4   period) within that entire basin, whilst we assume that floods between different basins

5   are independent of each other (Fraiture, 2007; Rojas et al., 2013). In the following

6   subsections, we describe the input flood hazard maps, the function fitting procedure,

7   and the Monte Carlo analysis in more detail.

8   ### 2.1.1 Input flood hazard maps

9   Our flood hazard data are extracted from the GLOFRIS global fluvial flood hazard

10   maps of Winsemius et al. (2013), which are developed using the GLOFRIS modelling

11   cascade provided in Ward et al. (2013) and Winsemius et al. (2013). The GLOFRIS

12   modelling cascade first simulates daily discharge using the PCRaster GlobalWater

13   Balance (PCR-GLOBWB) global hydrological model (Beek et al., 2008, 2011). Based on

14   daily discharge, daily flood volumes are simulated using the PCR-GLOBWB extension for

15   dynamic routing, DynRout (PCR-GLOBWB-DynRout) (Ward et al., 2013; Winsemius et

16   al., 2013). In the next step, flood volumes, for different return periods: 2, 5, 10, 25, 50,

17   100, 250, 500 and 1000 years, are obtained using the annual time series for maximum

18   flood volumes by fitting a Gumbel distribution. These flood volumes are then converted

19   into inundation maps (30-arcsecond, ca.1-km) using the inundation downscaling model

20   of GLOFRIS (Winsemius et al., 2013). In the appendix materials, we provide flood maps

1   for the 50 and 500-year return periods. The maps show that the inundation depth

2   highly varies in China. Railway lines in eastern coastal China and South China are faced

3   with the most severe floods.

4   We divide China into nine major river basins (Fig. 3) according to the main river

5   system from the Data Center for Resources and Environmental Sciences, Chinese

6   Academy of Sciences, which is accessible from the Resource and Environment Data

7   Cloud Platform (http://www.resdc.cn/, last access: 19 May 2020): the Continental Basin,

8   Haihe River Basin, Huaihe River Basin, Pearl River Basin, Songhua and Liaohe River Basin,

9   Southeast Basin, Southwest Basin, Yellow River Basin and Yangtze River Basin. As such,

10   we extract the flood hazard data for each of these river basins.

11   **2.1.2 Fitting procedure**

12   For each grid cell, the GLOFRIS maps estimate the flood depth for the nine

13   aforementioned return periods (2, 5, 10, 25, 50, 100, 250, 500 and 1000 years). To

14   estimate the flood depth for any return period, we fit a quadratic spline function to

15   develop an inundation depth-exceedance probability function (P) for each return period

16   interval for each grid cell (Marsden, 1974; Vandebogert, 2017; Meshram et al., 2018).

17   The quadratic spline is a method that uses a piecewise quadratic function to obtain the

18   best-fitting curves. This interpolation method allows us to obtain a smooth continuous

19   curve through the provided flood depths for the different return periods.

20   The method is applied as follows and examples of the inundation depth-exceedance

probability function of grid cells are shown in Fig. 2a:

For each grid cell $g_{x,y}$, the annual exceedance probability flood depth D_T is calculated by Eq. 1:

$$P(D_T) = \frac{1}{T} \qquad (1)$$

where D_T is the magnitude of a flood depth with return period of T-year, $P(D_T)$ is the exceedance probability of D_T. D_T is between $[D_1, D_{1000}]$, with $D_1 = D_2 \leq D_5 ... \leq D_{1000}$. We assume that D_1 is equal to zero (i.e., 1-year event with a flood depth of 0 m) and is the same as that of a 2-year event (the lowest return period in the GLOFRIS dataset). Let $Pr(D_T)$ denote a quadratic, continuously differentiable function of $P(D_T)$. Then, by definition:

$$Pr(D_T) = aD_T{}^2 + bD_T + c \qquad (2)$$

For each interval of grid cell $g_{x,y}$, we can obtain its piecewise quadratic function by Eq. 3:

$$Pr_{x,y}(D_T) = \begin{cases} Pr_{x,y}^1(D_T) = a_1 D_T{}^2 + b_1 D_T + c_1 & D_T \epsilon [D_2, D_5] \\ Pr_{x,y}^2(D_T) = a_2 D_T{}^2 + b_2 D_T + c_2 & D_T \epsilon [D_5, D_{10}] \\ \qquad \cdots \\ Pr_{x,y}^8(D_T) = a_8 D_T{}^2 + b_8 D_T + c_8 & D_T \epsilon [D_{500}, D_{1000}] \end{cases} \qquad (3)$$

where $Pr_{x,y}(D_T)$ is a set of continuous inundation depth-exceedance probability functions consisting of 8 continuous quadratic functions for $g_{x,y}$ and shows in Fig. 2a with curves. For $a(a_1, a_2, ..., a_8), b(b_1, b_2, ..., b_8), c(c_1, c_2, ..., c_8) \epsilon R$, we can calculate these constants by bracketing the critical point of $P(D_T)$ and derivative of the function $Pr_{x,y}(D_T)$; details on the interpolation methods can be found in a previous study by Sun and Yuan (2006). In this work, we assume that only one event occurs per year in

1   each basin since we assume the intensity of events is equal to or larger than 1-year.

2   When the return period is lower than 2, the flood depth is set to zero which is the same

3   as that of a 2-year event.

4   ### 2.1.3 Simulation procedure

5   To produce a time-series of flood events based on the created inundation depth-

6   exceedance probability functions (Section 2.1.2), we use a Monte Carlo sampling

7   method. The basic idea of the Monte Carlo sampling method is that when the number

8   of simulations is sufficiently large, the frequency of an event approximates the

9   probability of the occurrence of the event (Baker, 2008; Speight et al., 2017). The flood

10   event generation procedure is presented in Fig. 2 and Appendix Fig. A1 and can be

11   summarized in two steps. First, we generate independent events at each basin and

12   combined them into a national event. For an event E_j^i, and for each basin B_j, a random

13   number P_j^i between 0 and 1 is generated from a uniform distribution. The flood depth

14   of the cells in basin B_j for event E_j^i can be calculated using P_j^i and the inundation

15   depth-exceedance probability function based on the assumption that a flood event in

16   one basin will produce a flood with the same intensity. For a national-scale flood event,

17   basin-specific floods of nine basins can be randomly combined into a national-scale

18   flood by assuming independence between the flood events among different basins, this

19   concept is presented in Fig. 2b. Second, we repeat this process 10000 times to generate

20   a set of national-scale independent flood events as presented in Fig. 2c.
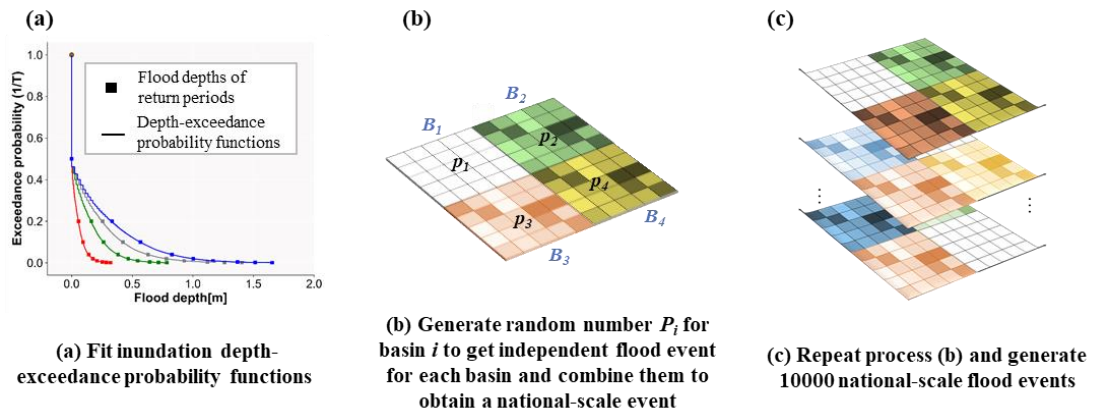
2 *Fig. 2 An example of generating national-scale flood events. In (b), p_1, p_2, p_3, and p_4*

3 *are the random number between 0 and 1 generated for basin B_1, B_2, B_3 and B_4, which*

4 *are used to generate basin-scale events based on the functions in (a). The layers of*

5 *basin-scale floods in (b) are combined into a national-scale flood event. The layers in (c)*

6 *are the 10000 national-scale events using the process in (b).*

7 For each year, we assume that within each basin, only one flood event can occur. For

8 each basin to obtain 10,000-year events (we assume that 10,000-year of events are

9 sufficient to cover almost all probable scenarios), we therefore apply a Monte Carlo

10 method to sample 10,000 exceedance probabilities. For each of these exceedance

11 probabilities, we estimate the inundation depth for each cell within that basin (i.e.,

12 assuming that the exceedance probability is the same throughout the entire basin). We

13 repeat this procedure for each basin, which results in a 10,000-year set of flood events

14 for each basin. We then combine these sets into a national scale flood event set by

15 assuming independence between the flood events in the different river basins (Fig. 2c).

16 Hence, for each of the 10,000 years, we simply take the estimated flood depths for each

17 basin. For example, in year 1, basin 1 may have an exceedance probability of 0.5, whilst

18 basin 2 may have an exceedance probability of 0.98. For year 1, the resulting national-

scale flood map would therefore have values for a flood event with an exceedance probability of 0.5 in basin 1, a flood event with an exceedance probability of 0.98 in basin 2, and so forth. This procedure results in a 10,000-year national-scale flood event set.

We also assess the system vulnerability by calculating the impacts that could occur throughout China if a flood with a given return period were to occur within an individual basin. To do this, for each basin and each return period we draw 10,000 events for all other basins assuming independence. In total, this leads to a set of 810,000 events (10,000 events x 9 return periods x 9 basins).

2.2 Railway network building

Railway systems are commonly represented through spatially explicit networks as an analogy for their structure and flows (Rodrigue, 2016). This network representation can be used to calculate system performance metrics based on network theory. In this work, the Chinese railway system was modelled as a directed weighted network, which consists of a group of nodes (stations) and connected by edges (railway lines) with daily train trips, where the edges have a travel direction associated with them. To build the Chinese railway network, we use the geographic information of railway system from OpenStreetMap (OSM) and the timetable data including daily number of trains and associated routes from the Railway Service Website (Liu et al., 2018a; Zhu et al., 2020). As our method is primarily concerned with flood risk along rail segments between cities

1   and not within cities, for simplicity, we combine multi-stations into one node using the

2   location of the highest capacity station in each city. In total, 2240 nodes are combined

3   into 1790 nodes. The final extracted railway network has a total length of 90,600 km for

4   (merged parallel) lines connecting two identical stations, consisting of 1973 edges and

5   1790 nodes (Fig. 3). Figure 3 shows the spatial distribution of the railway network and

6   average daily numbers of trains. Topology and traffic flows vary greatly in spatial apace.

7   The network density, reduces greatly moving from Eastern China to Western China. For

8   the traffic flow, the railways connect large cities, like the railways from Beijing to

9   Guangzhou, Harbin and Shanghai, and railway from Shanghai to Changsha have higher

10   flows.

12   *Fig. 3 The spatial distribution of the railway network and average daily numbers of trains.*

13   *The river basins layer comes from the Data Center for Resources and Environmental*

7   2.3 Failure condition based on an event

8   We assume that a railway is impassable when the water level on the railway line is

9   higher than the failure threshold Wd of the railway service after drainage (CRPH, 2012;

10 Espinet et al., 2018). The water level after drainage $WL_{x,y}$ of grid cell $g_{x,y}$ is

11 calculated by Eq. 4:

$$WL_{x,y} = D_{T_{x,y}} - Wld_{x,y} * Dc \tag{4}$$

13 where $D_{T_{x,y}}$ is the flood depth of a flood event, $Wld_{x,y}$ is the water level of the

14 design standard (i.e., the return period t) of grid cell $g_{x,y}$, and Dc is the drainage

15 capacity rate.

16 The rail segment l_{ij} between two stations failure condition is defined by Equations

17 5 and 6:

$$Fc_{ij} = \prod_{xy}^{ij} Z(xy) \tag{5}$$

$$Z(xy) = \begin{cases} 0, WL_{x,y} \geq Wd \\ 1, WL_{x,y} < Wd \end{cases} \tag{6}$$

20 Fc_{ij} is the failure condition of component l_{ij}, which has two states, namely, normal

21 (denoted by 1) and disrupted (denoted by 0), resulting in 100% disruption. $Z(xy)$ is

22 the failure condition of grid cell $g_{x,y}$; when the water level after drainage is larger than

1   Wd, $Z(xy)$=0; otherwise, $Z(xy)$=1.

2   In this study, we consider a failure threshold of 0.2 m after drainage, according to the

3   railway transportation emergency plan (CRPH, 2012; Espinet et al., 2018). The flood

4   design standard of the culverts, bridge and embankments of the Chinese national

5   railway system is designed for 100 year in China, according to the standard for flood

6   control (CRPH, 2016). Furthermore, we assume that the drainage capacity rate is 0.8 of

7   water level of the design standard, and it reduces the total amount of water that the

8   railway structure can actually drain (CRPH, 2016; Espinet et al., 2018).

9   Failure hotspots of railway segments l_{ij} can be found by the annual failure

10   probability AF_{ij}, which is calculated by Eq. 7:

$$AF_{ij} = \frac{\Sigma_e^E FC_{ij}^e}{N} \tag{7}$$

12   where AF_{ij} is the failure probability to the railway segments, E is the N-year flood

13   events catalogue, and FC_{ij}^e is the failure condition of railway segment l_{ij} under flood

14   event e.

15 ## 2.4 Performance loss metrics

16 ### 2.4.1 Daily affected trains and passengers

17   Once a flood occurs, trains may be affected in two ways: (i) increased travel time; or

18   (ii) cancellation. The number of daily affected trains N_e^{tol} is calculated by Eq. 8:

$$N_e^{tol} = N_e^c + N_e^d \tag{8}$$

20   Where N_e^c the number of daily is cancelled trains and N_e^d is the number of daily

1   detoured trains after a flood event.

2   We assume that the average number of passengers is 80% of the train's capacity

3   (Rezvani et al., 2015; Wei et al., 2017). As such, the number of affected passengers P_e^{tol}

4   can be defined by Eq. 9:

5 $$P_e^{tol} = \sum_i^{(N_e^c + N_e^d)} CA_i * 0.8 \tag{9}$$

6   where CA_i is the capacity of the ith train.

7 **2.4.2 Daily detoured trains and passengers influenced by detoured train**

8   Once a flood occurs, some trains will detour to complete their journeys. The daily

9   detoured trains N_e^d can be calculated based on four assumptions as follows (in order

10   of descending priority), which is also presented in Appendix Fig. A3:

11   ① Stations are not repeated along the routes;

12   ② The train passes the largest number of original stations along the detoured

13   route;

14   ③ The detour with the smallest increase in travel time is selected;

15   ④ Detouring is impossible when the increased time for re-routing is greater than

16   24 hours.

17   the daily passengers influenced by detoured train P_e^d can be defined by Eq. 10:

18 $$P_e^d = \sum_i^{(N_e^d)} CA_i * 0.8 \tag{10}$$

19   where N_d is the daily detoured trains and CA_i is the capacity of the ith train.

2.4.3 Total increased time for the detoured trains

The total increased time T_e^{tol} for detoured trains is calculated by Eq. 11:

$$T_e^{tol} = \sum_i^{N_d} T_i^e - \sum_i^{N_d} T_i \qquad (11)$$

where T_i^e is the running time of the ith train under flood event e, and T_i is the original travelling time of the ith train.

2.4.4 Average increased time for the detoured trains

The average increased time is calculated by Eq. 12:

$$T_e^{ave} = \frac{T_e^{tol}}{N_e^d} \qquad (12)$$

where T_e^{ave} is the average increased time under flood event e and N_d is the number of detoured trains.

2.4.5 Daily cancelled trains and passengers influenced by cancelled train

Once a flood occurs, some trains may be cancelled if there is no alternative route possible or when the re-routing time is too long (greater than 24 hours). The daily cancelled trains N_e^c is calculated by Eq. 13:

$$N_e^c = N_S - N_e^s \qquad (13)$$

where N_e^c is the daily cancelled trains after a flood event, N_e^s is the number of running trains in the system after a flood event, and N_S is the original number of trains in the system.

The daily passengers influenced by cancelled train P_e^c can be defined by Eq. 14:

$$P_e^c = \sum_i^{(N_e^c)} CA_i * 0.8 \qquad (14)$$

where N_c is the daily cancelled trains and CA_i is the capacity of the ith train.

2.5 Calculating system vulnerability and risk

Each performance loss metric is calculated for each flood event. System vulnerability curves are generated to present the relationship between performance loss and flood intensity (return period). We use the expected daily affected trains, cancelled trains, detoured trains, affected passengers and increased time for detoured trains to present the flood risk to the railway system according to Eq. 15:

$$AR_s = \frac{\Sigma_e^E V_e}{N} \qquad (15)$$

where AR_s is the expected daily flood risk level to the railway system, E is the N-event flood catalogue, and V_e is the performance loss metric, i.e., N_e^d, N_e^c, N_e^{tol}, P_e^d, P_e^c, P_e^{tol}, T_e^{tol}, and T_e^{ave} under flood event e, which is defined in Eqs. 9-14.

2.6 Uncertainty and sensitivity analysis

By applying an uncertainty analysis (UA), we identified the range of model output for imprecisely known input parameters (De Moel et al., 2012). A sensitivity analysis (SA) aims to determine the parameter effect on the model output (Koks and Haer, 2020). Parameters with greater effect should attract more additional attention to deal with the uncertainty they bring (Koks and Haer, 2020; De Moel et al., 2012). Detailed methods of uncertainty and sensitivity analysis can be found in previous studies by De Moel (2011) and Koks and Haer (2020).

1   In this study, we make assumptions on the train disruption threshold using three

2   parameters (the water level failure threshold, drainage capacity rate, and design

3   standard) based on emergency code and design code standards (CRPH 2012). However,

4   it should be noted that these standards are not known exactly for each asset and will

5   change over time, such as dynamically changing protection standards and ageing

6   infrastructure. Within a railway system, a lot of different asset types exist, with varying

7   design standards. This implies that the capacity to cope with the hazard does vary from

8   location to location. As such, it is worthwhile to perform a sensitivity analysis on these

9   key parameters (De Moel and Aerts, 2011; Horacio et al., 2019). Hence, we perform an

10   uncertainty and global sensitivity analysis in which we assess the performance loss

11   metrics for a range of different values for these parameters. For water level failure, we

12   use a range between 0.1 and 0.5 m. For the drainage capacity rate, we use a range

13   between 0.7 and 0.9, and for the design standards, we use a range between 50 and 100

14   years. The list of all assumptions taken in this study and their range in the sensitivity

15   analysis can be found in appendix Table A3. In total, we create a set of 1000 different

16   parameter value combinations in the sample space.

17   ## 3 Results

18   ## 3.1 Failure hotspots of railway segments

19   The annual failure probability of the network segments is shown in Fig. 4 and is

20   calculated based on the 10,000-year national flood event set. The results show a clear

1   regional differentiation (Fig. 4a). Areas with high annual failure probabilities are mainly

2   located in the Yangtze River Basin, Southeast Basin, and Pearl River Basin areas. These

3   three basins have a humid subtropical climate and high precipitation levels in the rainy

4   season during the summer; and these areas also have the highest railway density (Fig.

5   3), mostly across rivers and located on flat area in China, which makes these railway

6   lines susceptible to flood hazards.

7   Figure 4b shows the percentage of the length of railway lines that fall into each failure

8   probability category for the national- and basin-level analyses. Nationally, the failure

9   probability is greater than 0 for more than 55% of the total length of the railway lines.

10   This percentage is heterogeneous across different river basins: it is highest in the

11   Southeast Basin, followed by the Pearl River Basin and the Yangtze River Basin.

12   Nationally, 6.8% of the length of the railway lines has a failure probability greater than

13   0.02, with the highest proportions in the Yangtze River, Yellow River, and Southeast

14   Basins, with 12.5%, 10% and 7.2%, respectively. The results for the failure hotspots

15   indicate that the railways located in Yangtze River, Southeast and Pearl River Basins need

16   more attention and planned prevention measures to reduce the failure probability

17   induced by floods.
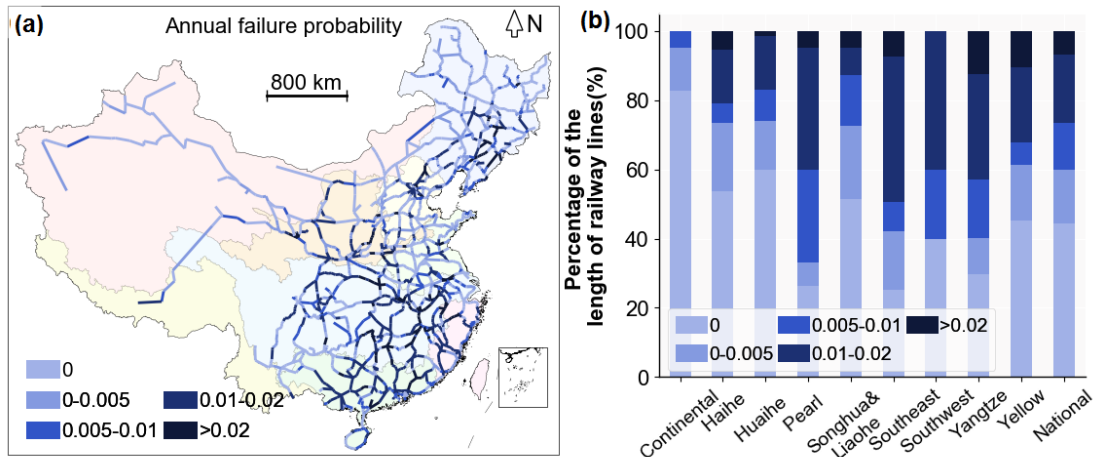
2 *Fig. 4 (a) Annual failure probability map of the network segments affected by floods and*

3 *(b) the percentage of the length of railway lines for different failure probability categories*

4 *per river basin. Railway geometries © OpenStreetMap contributors 2019. Distributed*

5 *under the Open Data Commons Open Database License (ODbL) v1.0.*

6 ## 3.2 Risk analysis of the Chinese railway system

7 The performance loss distribution curves of the railway system using the 10,000-year

8 national-scale flood set are presented in Fig. 5. The results show that approximately 85%

9 of the flood events have little effect (less than 0.01 of the daily trains and passengers) on

10 the railway system from the perspective of all the performance metrics. For the daily

11 affected trains, the absolute maximum number can reach 4200, and the average number

12 is approximately 200 trips; these values represent 59% and 2.7% of the number of the

13 daily trains. For the daily affected passengers, the absolute maximum number can reach

14 3,500,000, and the average number is approximately 165,000 people (60% and 2.8 of the

15 number of the daily passengers). In addition, the largest average increased time for detoured

16 trains can reach 14 hours and the mean average increased time for detoured trains is

1   approximately 5 hours.
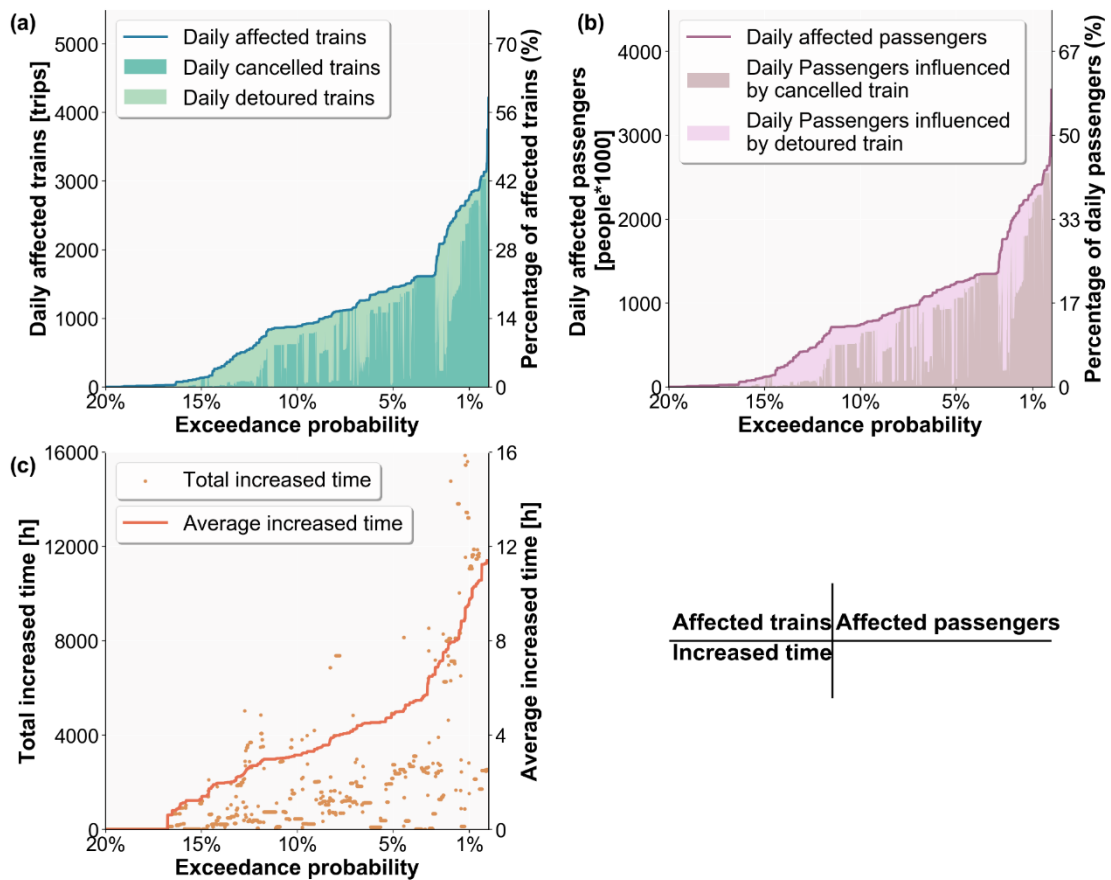
3   *Fig. 5 Exceedance probability-performance loss curves*

4   The performance losses per province of the railway system are presented in Fig. 6 for

5   a range of metrics. The risk differs considerably between regions when expressed in

6   different risk metrics. When examining the metrics of the daily affected trains and

7   affected passengers, we find that the provinces in Central China, such as Henan, Hubei

8   and Anhui, have the highest absolute and relative risks, estimated to be over 40 daily

9   affected trains (4.5% relative to the number of the province's daily trains) and more

10   than 35,000 daily affected passengers (3.5% relative to the number of the province's

11   daily passengers). Interestingly, some provinces, such as Tibet Province, have a low risk

1   in absolute terms but a high risk in relative terms because the Tibet Province has the

2   smallest rail network and rail traffic density; only one line (i.e., Qinghai-Tibet Railway)

3   crosses this region, which is therefore highly vulnerable to even a low-frequency flood

4   hazard. Guangdong Province has the opposite results, with high risk in absolute terms

5   and low risk in relative terms due to the large rail network and rail traffic density, which

6   make the railway system more robust even with a high flood failure probability. The total

7   and average increased time for detoured trains show contrasting results. The high risk

8   in terms of the total increased time is mostly distributed in East China, whereas the

9   highest average increased time is distributed in western provinces such as Xinjiang and

10   Tibet Provinces. From Eastern China to Western China, the traffic flow becomes

11   significantly lower; more trains can be detoured with less time per trip in East China,

12   and in the western provinces, fewer trains can be detoured but with more time per trip.
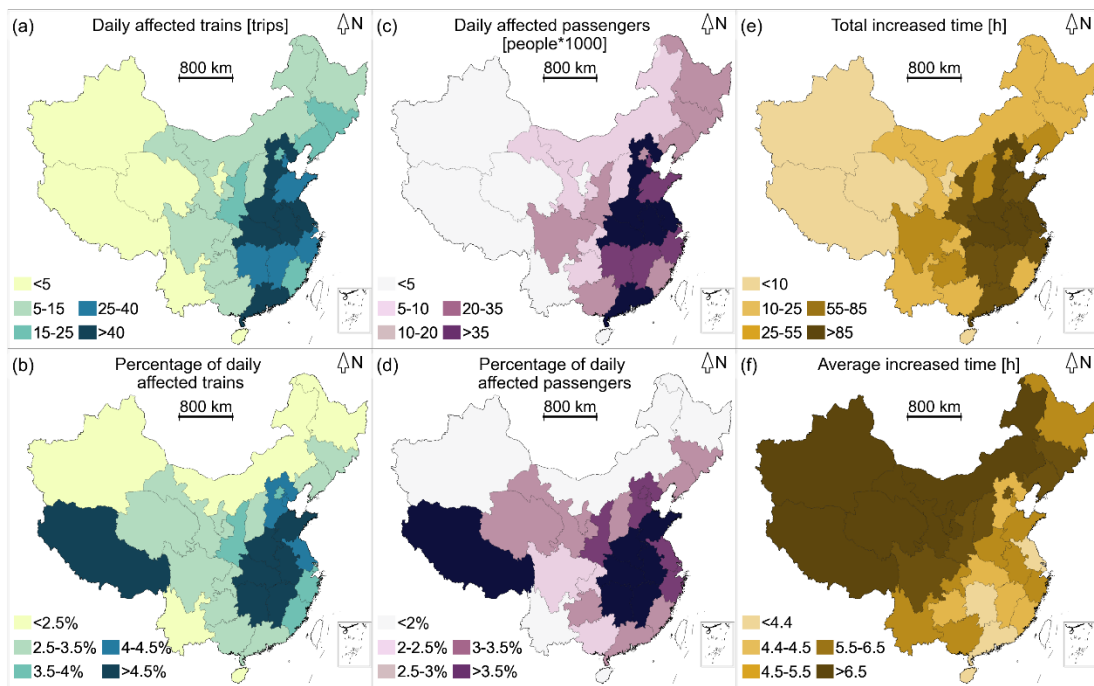
Fig. 6 Performance loss of the railway system per province. (a) The daily affected trains in absolute terms; (b) the daily affected trains relative to the number of the province's daily trains; (c) the daily affected passengers in absolute terms; (d) the daily affected passengers relative to the number of the province's daily passengers; (e) the daily total increased time for the detoured trains per province; and (f) daily average increased time for the detoured trains per province. Appendix Fig. A4 provides the risk map of detoured and cancelled trains and passengers influenced by detoured, cancelled train. Appendix Fig. A5 provides a map of the Chinese provinces

Several provinces appear at the highest level of the three metrics presented in Fig. 6 and can be classified as particularly vulnerable provinces. Anhui Province, for example, has one of the highest absolute and relative levels of risk to trains and passengers in Fig. 6a-d but also has the highest total increased time in Fig. 6e. Hubei Province shows one of the highest absolute and relative levels of risk to trains and passengers in Fig. 6a-d. Jiangsu Province has the highest absolute levels of risk to trains and passengers in Fig. 6a and c and one of the highest total increased time in Fig. 6e. These provinces are at

1 the highest risk compared to the other provinces. This information can help researchers

2 and local authorities to determine high-risk areas and prioritize hazard-risk

3 management interventions to reduce risk. These can be used in the first steps of

4 developing climate-resilient infrastructure.

3.3 System vulnerability of the Chinese railway system

6 Figure 7 presents system vulnerability curves based on the 810,000 simulated flood

7 events and shows the performance loss metrics (namely, the percentage of daily

8 affected trains and increased time) plotted against the return periods. The bottom-right

9 plots for subfigures a and b show the national results, whilst the other figures show the

10 results for each river basin. The colour shade represents the distribution of the flood

11 performance loss, where the lines refer to the median performance loss value and the

12 bounded lines refer to the 10th and 90th percentiles. The low-impact events cause the

13 median values to be the same as the lower bound for the nine river basins as a result

14 of their high frequency.
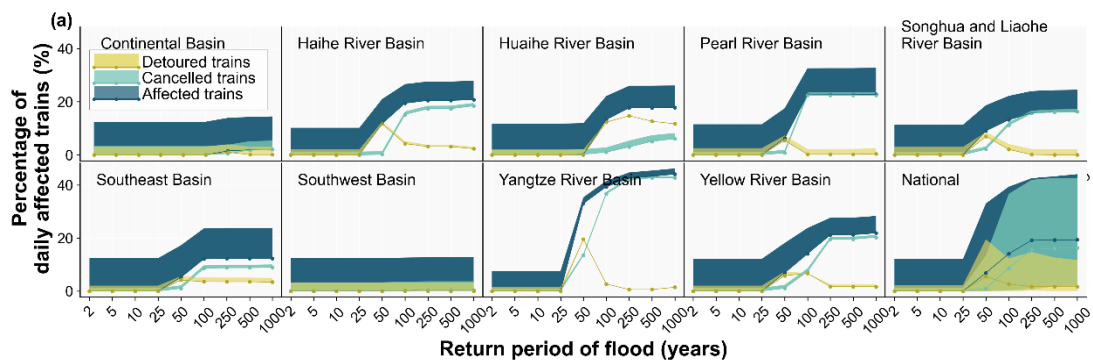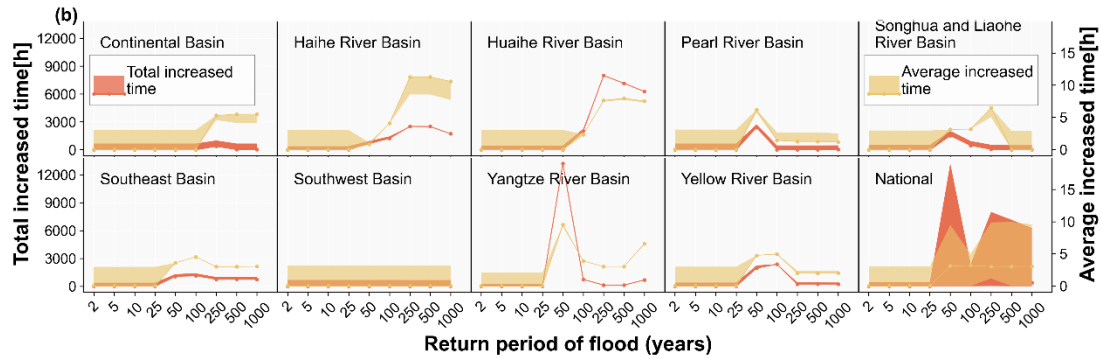
2   *Fig. 7 System vulnerability curves induced by river floods from the national flood event*

3   *set, showing: (a) the percentage of daily affected trains to the total number of daily trains*

4   *and; (b) the increased time for the detoured trains. The shading shows the distribution of*

5   *the flood performance loss, where the lines refer to the median performance loss value*

6   *and the bounded lines refer to the 10th and 90th percentiles. In the Appendix Fig. A6, we*

7   *provide the system vulnerability curves for the passenger-level metrics. NB: for total*

8   *increased travel time, the values can decrease at higher return periods – this is because*

9   *some of the trains are cancelled and therefore there is no travel time for those trains*

10   Due to the different definitions and focus of each metric, the relationship between

11   each metric and flood intensity is also different. From Fig. 7a, we can see that the

12   percentage of daily affected trains and daily cancelled trains to the total number of daily

13   trains increases with the increases of the return period of the flood events for the nine

14   basins. The percentage of daily detoured trains to the total number of daily trains and

15   the total and average increased time for detoured trains do not always increase with

16   increasing return period shown in Fig. 7a and Fig. 7b. The median performance loss for

17   the five metrics is close to zero for floods with a return period below 25-years and

18   remains stable when the flood hazard return period exceeds 100-years because of the

19   railway design protection standards and assumed drainage capacity. Between the 25-

year and 100-year flood events, the percentage of daily affected trains and daily

cancelled trains relative to the total number of daily trains per flood event increases.

The percentage of daily detoured trains relative to total daily trains and the total and

average increased time, increases between the 25-year and 50-year flood events, and

sharply decreases between the 50-year and 100-year events, especially for the Yangtze

River, Yellow River and Pear River Basin floods. This is because most of the north-south

rail lines in China, such as the Beijing-Guangzhou and Beijing-Jiulong lines, cross these

basins. Most trains that are detoured for a 50-year event cannot be detoured for a 100-

year event, as most of the north-south rail lines suffer failures at this hazard intensity.

When comparing the results between the nine river basins, we find that, in general,

floods in the basins in central and eastern China have the highest impacts on the

Chinese national railway system. The percentage of daily affected trains (cancelled and

detoured trains) of the total number of trains is the largest for the Yangtze River Basin,

followed by the Pearl River Basin and the Yellow River Basin. In the Yangtze River Basin,

the median percentage of daily affected trains (cancelled and detoured trains) to the

total number of trains is close to 40% for a 100-year flood event. For the Continental

and Southwest Basins, the value is close to zero. The high impacts of daily affected trains

observed in the central and eastern area are due to a significantly higher railway line

density and daily train flows compared to the more inland river basins (see Fig. 3). The

higher annual failure probability of the rail segments in the central and eastern regions

shown in Fig. 4 also leads to a higher probability of failed railway segments per flood

1 event and results in higher impact. The daily detoured trains in the Huaihe and Haihe

2 River Basins in eastern China are higher compared to other basins, which leads to a

3 large total increased time when one flood occurs. The reason is that the Huaihe and

4 Haihe River Basins are located in eastern China and only cross railway lines in the

5 eastern coastal area. Therefore, the affected trains have more detour options through

6 the lines of the Yangtze and Yellow River Basins, which lead to more detoured trains and

7 associated total increased time. For each basin, based on the vulnerability curve, once

8 we know the intensity of flooding that would occur, we can estimate the affected trains

9 and passengers. Based on this kind of information, local authorities could prepare

10 dispatch plans in advance of floods.

11 ## 3.4 Risk uncertainty and parameters sensitivity

12   Figure 8 and Appendix Fig. A7 present the sensitivity of the results to the assumed

13 parameters and the range of performance metric uncertainty. Overall, from the

14 uncertainty histograms, we can see that all the performance metrics are right-skewed,

15 especially for the average daily affected and affected passengers shown in Fig. 8a and c,

16 and average daily cancelled trains and passengers influenced by cancelled train shown

17 in Appendix Fig. A7b and d, have a long right tail for high performance loss estimates.

18 This seems a little bit less for the average daily detoured trains and passengers

19 influenced by detoured train shown in Appendix Fig. A7a and c, and average increased

20 time for detoured trains showed in Fig. 8e, which is probably the result of the

1   assumption that detouring is impossible when the increased time for re-routing is

2   greater than 24 hours, resulting in a smaller range of detoured options and thus a

3   smaller range in resulting performance loss estimates. The average number of daily

4   affected trains ranges from 100 to 500 trips. For daily affected passengers, it ranges

5   between 100,000 and 450,000 people, and the average increased time ranges between

6   3.5 hours and 5.5 hours with the change in the parameters.

7   In Fig. 8b, d, f and Fig. A7f, the pie-charts show how much the uncertainty in each

8   input parameter contributes to the variance of the performance loss estimates. The

9   results show that the performance loss estimates are particularly sensitive to the values

10   used for the design standards. Using the different parameter settings, we see a variation

11   in the design standards of approximately 43%. The variation in the drainage capacity

12   rate and water level threshold produces similar uncertainty as the capacity loss, which

13   is approximately 28%. Reducing uncertainty in risk assessment is particularly

14   challenging as it would require location-specific parameters. Despite the difficulties,

15   these geographically varying design standards should be developed in the future to

16   reduce uncertainty and improve the performance loss estimates.
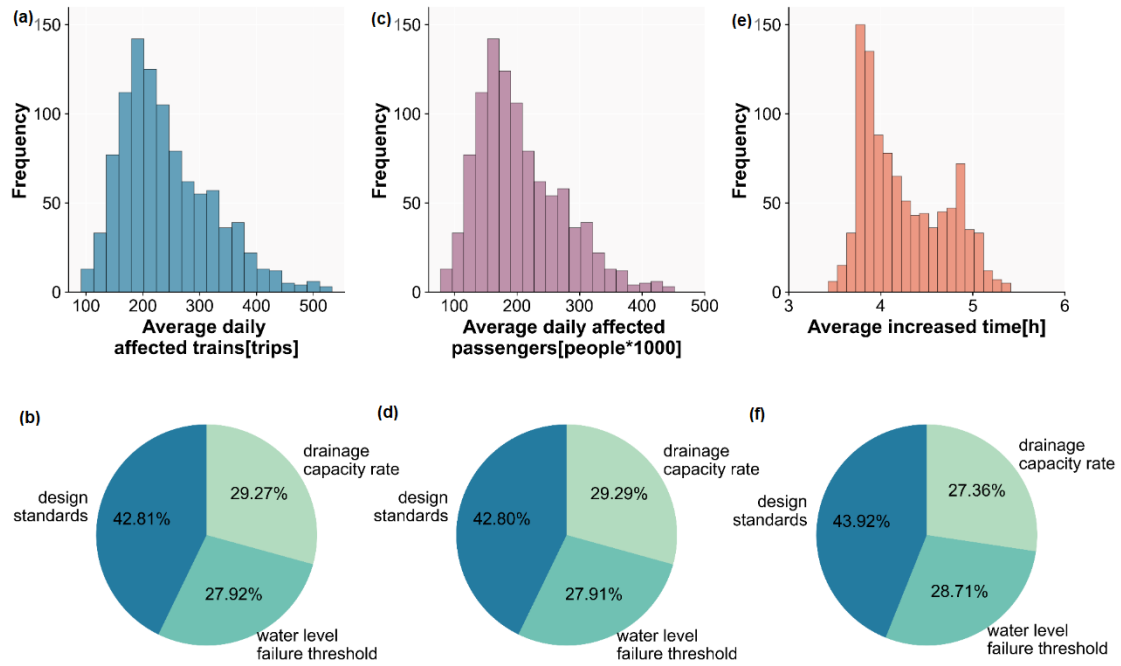
2 *Fig. 8 Results of the uncertainty (histograms) and sensitivity (pie charts) analyses for the*

3 *performance metrics. (a) and (b) average daily affected trains; (c) and (d) average daily*

4 *affected passengers; (d) and (f) average increased time. Fig. A7 provides the results of*

5 *the other performance metrics.*

6 ## 4 Discussion

7   Our results reveal clear geographical disparities in the failure hotspots. Areas with

8 high annual failure probabilities are mainly located in the Yangtze River Basin, Southeast

9 Basin, and Pearl River Basin. Comparing the failure probability from this study with the

10 susceptibility map presented in seminal works by Liu et al. (Liu et al., 2018a, 2018b), we

11 find some differences in hotspots in Xinjiang Province and along the Beijing-Shanghai

12 line. In our study, we find lower failure probabilities relative to the work of Liu et al. For

13 other regions, the spatial patterns are similar. Our study considers the same protection

14 standards (the water level failure threshold, drainage capacity rate, and design standard)

1   for the railway lines in the Chinese railway system. It should be noted that these

2   standards will not remain constant over time, as a result of ageing infrastructure. This

3   means that the failure probability in some areas in this study is biased compared to

4   research based on historical data. Indeed, many older lines have been

5   upgraded/improved so that the protection standards are more consistent with newer

6   lines.

7   In our work, we find that in the Yangtze River Basin, the median relative cancelled

8   trains to total daily trains is between 0 and 14% when the flood intensity is between 25

9   and 50-year. In 2016, from May to July, the Yangtze River Basin and Huaihe River Basin

10   suffered by severely rainfall (Lyu et al., 2018). In most affected areas within the Yangtze

11   River Basin, the floods that occurred exceeded the 25-year return period. Floods caused

12   disruptions on several railway lines, including the Chengdu-Chongqing line, Hefei-

13   Jiujiang line, and Sichuan-Guizhou line, that cross the Yangtze River Basin. In the Huaihe

14   River Basin, damage occurred to the Beijing-Guangzhou line. From 30 June to 6 July,

15   approximately 100 trips (approximately 2% of the daily trains) were cancelled every day

16   for the Chinese railway system. These observed impacts are within the range of our

17   estimates.

18   In this study, we assumed that within a river basin, the flood probability is constant,

19   whilst among different basins it is fully independent. In future work, we will assess the

20   dependence structure of flood hazards within and between basins, for example, by

21   means of the copula approach as presented in (Jongman et al., 2014). As we assumed

1   a disruption time of one day due to the lack of information on flood duration in this

2   study, we may have underestimated the operational performance losses.

3   In the broader context of risk assessments for transportation systems, the simplified

4   method for generating independent flood events offers a practical method for the large-

5   scale assessment of performance losses and indirect risk. Most existing studies used

6   regional- or national-scale flood footprints to assess flood-induced risk. However, in

7   reality the floods shown in such a flood footprint would not all happen at the same time.

8   For comparison, we calculated the performance loss for the Chinese railway system

9   using national-scale flood footprints (2, 5, 10, 25, 50, 100, 250, 500 and 1000 years in

10   whole China) as shown in Fig. 9 a) and b). Results show that the performance loss for

11   both affected train trips and passengers is almost unaffected for national-scale flood

12   footprints with a return period below 25-years. However, performance loss sharply

13   increases when the flood hazard return period exceeds 50-years. More than 90% of

14   trains and passengers would be affected when the flood hazard return period exceeds

15   100-years. Compared with the performance loss obtained using the generated

16   independent flood events, the results using the national-scale flood footprints are

17   underestimated for small intensity flood events and overestimated for large intensity

18   flood events. Therefore, when assessing possible cascading effects, the use of

19   independent flood events is necessary (Nones and Pescaroli, 2016).
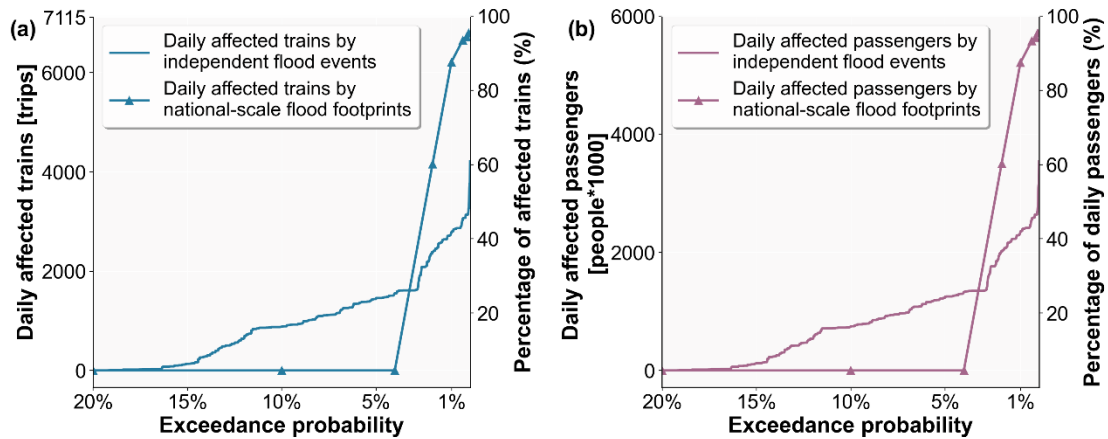
Fig. 9 performance loss for the Chinese railway system using national-scale flood

footprints (a) daily affected trains and (b) daily affected passengers

5   Conclusion

The increased frequency of extreme flood events, coupled with interregional trade

growth, requires national- and global-scale transportation networks to be more resilient

to cope with disruptive events. Evaluation of system-level vulnerability and

identification of risk hotspots is a first step to enhance the robustness of the transport

system. This study presents a framework for performing system-level vulnerability and

risk assessments of a railway system under flooding. The developed framework couples

simulated flood events with state-of-the-art network analysis to measure system

disruptions caused by floods to identify risk hotspots. This work quantifies the system

vulnerability and risk in terms of the performance loss of the Chinese railway system,

induced by the flooding. Results show that failure hotspots, system vulnerability and

the risk of the Chinese railway system under floods are highly heterogeneous. In

addition, the adopted vulnerability metrics present different results in terms of the

1   system vulnerability and risk.

2   High failure hotspots are mainly distributed in South China, i.e. Yangtze River, Pearl

3   River and Southeast Basins. The humid subtropical climate and severe flood hazards in

4   these areas result in large chances of disruption. For the system vulnerability, the

5   heterogeneity is largely due to a spatially imbalanced railway topology and traffic flow

6   as well as a spatially heterogeneous hazard intensity distribution among China. In

7   general, floods in the basins in central and eastern China have the highest impacts on

8   the Chinese railway system. Floods in the Yangtze River Basin have the largest impact

9   on the daily cancelled trains and daily passengers influenced by cancelled train. In the

10   Yangtze River Basin, the median percentage of daily affected trains to the total number

11   trains can reach to 45% for a 1000-year flood event. In addition, floods in the Huaihe

12   and Haihe River Basins cause the largest number of the detoured trains as well as

13   associated increased time for the Chinese railway system compared with other basins.

14   Finally, this work quantifies the performance risk due to flooding at the national and

15   provincial level. We find that, at a national level, the average daily number of affected

16   trains and passengers are approximately 200 trips and 165,000 people (2.7% and 2.8%

17   of the total daily numbers of trains and passengers), respectively. The mean average

18   increased time for detoured trains reaches approximately 5 hours. At the provincial

19   level, the provinces in Central China have the highest absolute and relative risks,

20   estimated to be over 40 daily affected trains (4.5% relative to the number of the

21   province's daily trains) and more than 35,000 daily affected passengers (3.5% relative

to the number of the province's daily passengers). The high risk in terms of the total increased time is mostly distributed in East China, whereas the highest average increased time is distributed in western provinces, such as Xinjiang and Tibet Provinces. The developed system vulnerability curves and flood risk maps can provide the information for the decisions on safety and effectiveness of operation and maintenance. Various performance metrics can be considered by management departments based on their particular problems.

The developed system vulnerability curves and flood risk maps can provide information for decisions on safety and effectiveness of operation and maintenance. Various performance metrics can be considered by management departments based on their particular problems. Using our current approach, the performance loss can be used as the start of the indirect risk assessment from the travel journey perspective. By combining the ticket prices and the operating cost per kilometre, the economic loss for the railway company can be calculated based on the affected trains and associated passengers (Lamb et al., 2019). As a key mode of transport for interregional trade, the failure of railway systems can produce large shocks for industries that depend on the supply that may come from flooded businesses. The risk values per province (such as expected daily cancelled trains and passengers influenced by cancelled train) can be used as indicators to link with business disruptions. Future work can try to assess the interregional trade based on Input and Output table and regional railway transportation performance decreased in our work. The assessment of shocks and indirect economic

1 losses induced by railway system failures is essential for policymakers to design railway

2 infrastructures and to measure indirect economic losses.

Code/Data availability

5 Supporting data are accessible through the associated reference. The data in this study

6 were analysed with Python package, and the figures were created with ArcViewTM GIS

7 and Python packages. All codes used in this work are available upon request.

Author contribution

9 Kai Liu and Weihua Zhu developed the original idea and designed the analyses. Philip

10 Ward and Elco Koks contributed to the study design. Weihua Zhu, Kai Liu and Elco Koks

11 conducted the analysis. Weihua Zhu wrote the original manuscript, and Kai Liu, Ming

12 Wang, Philip Ward and Elco Koks provided comments and revised the manuscript. All

13 the co-authors contributed to scientific interpretations of the results.

Declaration of Competing Interest

15 The authors declare that they have no known competing financial interests or personal

16 relationships that could have appeared to influence the work reported in this paper.

Acknowledgments

18 This work was supported by the National Key Research and Development Plan [grant

19 number 2018YFC1508802]; the National Natural Science Foundation of China [grant

number 41771538]; and PJW received funding from the Dutch Research Council (NWO), in the form of a VIDI grant [grant number 016.161.324]. EEK received funding from the Dutch Research Council (NWO), in the form of a VENI grant [grant number VI.Veni.194.033]. The financial support is highly appreciated.

References

Alfieri, L., Burek, P., Dutra, E., Krzeminski, B., Muraro, D., Thielen, J. and Pappenberger, F.: GloFAS-global ensemble streamflow forecasting and flood early warning, Hydrol. Earth Syst. Sci., 17(3), 1161–1175, doi:10.5194/hess-17-1161-2013, 2013.

Arnell, N. W. and Gosling, S. N.: The impacts of climate change on river flood risk at the global scale, Clim. Change, 134(3), 387–401, doi:10.1007/s10584-014-1084-5, 2016.

Baker, J. W.: An introduction to probabilistic seismic hazard analysis(PSHA), White Paper, Version 1.3., 2008.

Becker, A. and Grünewald, U.: Flood Risk in Central Europe, Science (80-.)., 300(5622), 1099, 2003.

Beek, L. P. H. (Rens) van, Bierkens, M. F. P. and Department: The Global Hydrological Model PCR-GLOBWB : Conceptualization , Parameterization and Verification Department of Physical Geography Faculty of Earth Sciences, Rep. Dep. Phys. Geogr. Utr. Univ. Utrecht, Netherlands, 2008.

Beek, L. P. H. Van, Wada, Y. and Bierkens, M. F. P.: Global monthly water stress : 1 . Water balance and water availability, , 47(April), doi:10.1029/2010WR009791, 2011.

Benn, J.: Railway bridge failure during flooding in the UK and Ireland, Proc. Inst. Civ. Eng. Eng., 166(4), 163–170, 2013.

Chang, H., Lafrenz, M., Jung, I. W., Figliozzi, M., Platman, D. and Pederson, C.: Potential impacts of climate change on Flood-Induced Travel Disruptions: A Case Study of Portland, Oregon, USA, Ann. Assoc. Am. Geogr., 100(4), 938–952, doi:10.1080/00045608.2010.497110, 2010.

CRPH: High-speed railway emergency response plan., 2012.

CRPH: Code for design of railway earth structure, TB10001, 2016.

Dottori, F., Salamon, P., Bianchi, A., Alfieri, L., Hirpa, F. A. and Feyen, L.: Development and evaluation of a framework for global flood hazard mapping, Adv. Water Resour., 94, 87–102,

1   doi:https://doi.org/10.1016/j.advwatres.2016.05.002, 2016.

2   Editorial Board of China Railway Yearbook, Ed.: China railway yearbook, China Railway Publishing House, Beijing.,

3   2001.

4   Editorial Board of China Railway Yearbook, Ed.: China railway yearbook, China Railway Publishing House, Beijing.,

5   2002.

6   Editorial Board of China Railway Yearbook, Ed.: China railway yearbook, China Railway Publishing House, Beijing.,

7   2003.

8   Editorial Board of China Railway Yearbook, Ed.: China railway yearbook, China Railway Publishing House, Beijing.,

9   2004.

10   Editorial Board of China Railway Yearbook, Ed.: China railway yearbook, China Railway Publishing House, Beijing.,

11   2005.

12   Editorial Board of China Railway Yearbook, Ed.: China railway yearbook, China Railway Publishing House, Beijing.,

13   2006.

14   Editorial Board of China Railway Yearbook, Ed.: China railway yearbook, China Railway Publishing House, Beijing.,

15   2007.

16   Editorial Board of China Railway Yearbook, Ed.: China railway yearbook, China Railway Publishing House, Beijing.,

17   2008.

18   Editorial Board of China Railway Yearbook, Ed.: China railway yearbook, China Railway Publishing House, Beijing.,

19   2009.

20   Editorial Board of China Railway Yearbook, Ed.: China railway yearbook, China Railway Publishing House, Beijing.,

21   2010.

22   Editorial Board of China Railway Yearbook, Ed.: China railway yearbook, China Railway Publishing House, Beijing.,

23   2011.

24   Editorial Board of China Railway Yearbook, Ed.: China railway yearbook, China Railway Publishing House, Beijing.,

25   2012.

26   Editorial Board of China Railway Yearbook, Ed.: China railway yearbook, China Railway Publishing House, Beijing.,

27   2013.

1 Editorial Board of China Railway Yearbook, Ed.: China railway yearbook, China Railway Publishing House, Beijing.,
2 2014.

3 Editorial Board of China Railway Yearbook, Ed.: China railway yearbook, China Railway Publishing House, Beijing.,
4 2015.

5 Editorial Board of China Railway Yearbook, Ed.: China railway yearbook, China Railway Publishing House, Beijing.,
6 2016.

7 Editorial Board of China Railway Yearbook, Ed.: China railway yearbook, China Railway Publishing House, Beijing.,
8 2017.

9 Espinet, X., Rozenberg, J., Ogita, K. S. R. S., Singh Rao, K. and Ogita, S.: Piloting the Use of Network Analysis and
10 Decision-Making under Uncertainty in Transport Operations: Preparation and Appraisal of a Rural Roads Project in
11 Mozambique Under Changing Flood Risk and Other Deep Uncertainties., 2018.

12 Fraiture, C.: Integrated water and food analysis at the global and basin level. An application of WATERSIM, WATER
13 Resour. Manag. -DORDRECHT-, 2007.

14 GFDRR: Tbilisi disaster needs assessment 2015., 2015.

15 Gil, J. and Steinbach, P.: From flood risk to indirect flood impact: Evaluation of street network performance for
16 effective management, response and repair, WIT Trans. Ecol. Environ., 118, 335–344, doi:10.2495/FRIAR080321,
17 2008.

18 Gong, M., Wang, Y., Wang, S. and Liu, W.: Enhancing robustness of interdependent network under recovery based
19 on a two-layer-protection strategy, Sci. Rep., 7(1), 1–13, doi:10.1038/s41598-017-13063-2, 2017.

20 Gouldby, B. and Samuels, P. G.: Title Language of Risk - Project definitions Technical Report, , (May 2014), 2009.

21 Haimes, Y. Y.: On the complex definition of risk: A systems-based approach, Risk Anal., 29(12), 1647–1654,
22 doi:10.1111/j.1539-6924.2009.01310.x, 2009.

23 Hirabayashi, Y., Mahendran, R., Koirala, S., Konoshima, L., Yamazaki, D., Watanabe, S., Kim, H. and Kanae, S.: Global
24 flood risk under climate change, Nat. Clim. Chang., 3(9), 816–821, doi:10.1038/nclimate1911, 2013.

25 Hong, L., Ouyang, M., Peeta, S., He, X. and Yan, Y.: Vulnerability assessment and mitigation for the Chinese railway
26 system under floods, Reliab. Eng. Syst. Saf., 137(January 2018), 58–68, doi:10.1016/j.ress.2014.12.013, 2015.

27 Horacio, J., Ollero, A., Noguera, I. and Fernández-Pasquier, V.: Flooding, channel dynamics and transverse

infrastructure: a challenge for Middle Ebro river management, J. Maps, 5647, doi:10.1080/17445647.2019.1592719, 2019.

Janic, M. and Vleugel, J.: Estimating potential reductions in externalities from rail–road substitution in Trans-European freight transport corridors, Transp. Res. Part D Transp. Environ., 17(2), 154–160, doi:https://doi.org/10.1016/j.trd.2011.09.015, 2012.

Jongman, B., Hochrainer-Stigler, S., Feyen, L., Aerts, J. C. J. H., Mechler, R., Botzen, W. J. W., Bouwer, L. M., Pflug, G., Rojas, R. and Ward, P. J.: Increasing stress on disaster-risk finance due to large floods, Nat. Clim. Chang., 4(4), 264–268, doi:10.1038/nclimate2124, 2014.

Kellermann, P., Schöbel, A., Kundela, G. and Thieken, A. H.: Estimating flood damage to railway infrastructure - The case study of the March River flood in 2006 at the Austrian Northern Railway, Nat. Hazards Earth Syst. Sci., 15(11), 2485–2496, doi:10.5194/nhess-15-2485-2015, 2015.

Kellermann, P., Schönberger, C. and Thieken, A. H.: Large-scale application of the flood damage model RAilway Infrastructure Loss (RAIL), Nat. Hazards Earth Syst. Sci., 16(11), 2357–2371, doi:10.5194/nhess-16-2357-2016, 2016.

Koks, E. E. and Haer, T.: A high-resolution wind damage model for Europe, Sci. Rep., 10(1), 1–11, doi:10.1038/s41598-020-63580-w, 2020.

Koks, E. E., Rozenberg, J., Zorn, C., Tariverdi, M., Vousdoukas, M., Fraser, S. A., Hall, J. W. and Hallegatte, S.: A global multi-hazard risk analysis of road and railway infrastructure assets, Nat. Commun., 10(1), 1–11, doi:10.1038/s41467-019-10442-3, 2019.

Kundzewicz, Z., IwonaPińskwar and Robertbrakenridge, G.: Large floods in Europe, 1985–2009, Int. Assoc. Sci. Hydrol. Bull., 2013.

Lamb, R., Garside, P., Pant, R. and Hall, J. W.: A Probabilistic Model of the Economic Risk to Britain's Railway Network from Bridge Scour During Floods, Risk Anal., doi:10.1111/risa.13370, 2019.

Lavers, D. A., Allan, R. P., Villarini, G., Lloydhughes, B., Brayshaw, D. J. and Wade, A. J.: Future changes in atmospheric rivers and their implications for winter flooding in Britain, Environ. Res. Lett., 8(3), 34010, 2013.

Liu, K., Wang, M., Cao, Y., Zhu, W., Wu, J. and Yan, X.: A comprehensive risk analysis of transportation networks affected by rainfall-Induced multihazards, Risk Anal., 38(8), 1618–1633, doi:10.1111/risa.12968, 2018a.

Liu, K., Wang, M., Cao, Y., Zhu, W. and Yang, G.: Susceptibility of existing and planned Chinese railway system

subjected to rainfall-induced multi-hazards, Transp. Res. Part A Policy Pract., 117, 214–226, 2018b.

Lyu, H. M., Xu, Y. S., Cheng, W. C. and Arulrajah, A.: Flooding hazards across Southern China and prospective sustainability measures, Sustain., 10(5), 1–18, doi:10.3390/su10051682, 2018.

Marsden, M. J.: Quadratic spline interpolation, Bull. Am. Math. Soc., 80(5), 903–906, doi:10.1090/S0002-9904-1974-13566-4, 1974.

Meshram, S. G., Powar, P. L. and Meshram, C.: Comparison of cubic, quadratic, and quintic splines for soil erosion modeling, Appl. Water Sci., 8(6), 1–7, doi:10.1007/s13201-018-0807-6, 2018.

Metropolis: The beginning of the Monte Carlo method, Cambridge Press. 1638-1692, 1–20, doi:10.9783/9781512808797-001, 1987.

De Moel, H. and Aerts, J. C. J. H.: Effect of uncertainty in land use, damage models and inundation depth on flood damage estimates, Nat. Hazards, 58(1), 407–425, doi:10.1007/s11069-010-9675-6, 2011.

De Moel, H., Asselman, N. E. M. and H. Aerts, J. C. J.: Uncertainty and sensitivity analysis of coastal flood damage estimates in the west of the Netherlands, Nat. Hazards Earth Syst. Sci., 12(4), 1045–1058, doi:10.5194/nhess-12-1045-2012, 2012.

Moran, A. P., Thieken, A. H., Schöbel, A. and Rachoy, C.: Documentation of flood damage on railway infrastructure, Data Mobility, pp. 61-70. Springer, Berlin, Heidelb., 81, 61–70, doi:10.1007/978-3-642-15503-1_6, 2010.

Newman, M. E. .: Networks An Introduction, Oxford University Press, United States., 2010.

Nones, M. and Pescaroli, G.: Implications of cascading effects for the EU Floods Directive, Int. J. River Basin Manag., 14(2), 195–204, doi:10.1080/15715124.2016.1149074, 2016.

Pregnolato, M., Ford, A., Wilkinson, S. M. and Dawson, R. J.: The impact of flooding on road transport: A depth-disruption function, Transp. Res. Part D Transp. Environ., 55, 67–81, doi:10.1016/j.trd.2017.06.020, 2017.

Prudhomme, C. and Genevier, M.: Can atmospheric circulation be linked to flooding in Europe?, Hydrol. Process., 25(7), 1180–1190, doi:10.1002/hyp.7879, 2011.

Reed, D. W.: A review of British railway bridge flood failures, Hydrol. Sci. Pract. 21st Century, I, 210–216 [online] Available from: https://www.researchgate.net/profile/Duncan_Reed/publication/267254265_A_review_of_British_railway_bridge_flood_failures/links/5512efd60cf240060b2df24c.pdf, 2004.

Rezvani, Z., Jansson, J. and Bodin, J.: Advances in consumer electric vehicle adoption research: A review and research agenda, Transp. Res. Part D Transp. Environ., 34, 122–136, doi:10.1016/j.trd.2014.10.010, 2015.

Rodrigue, J.-P.: The geography of transport systems, Taylor & Francis., 2016.

Rojas, R., Feyen, L. and Watkiss, P.: Climate change and river floods in the European Union: Socio-economic consequences and the costs and benefits of adaptation, Glob. Environ. Chang., 23(6), 1737–1751, doi:10.1016/J.GLOENVCHA.2013.08.006, 2013.

Sampson, C. C., Smith, A. M., Bates, P. D., Neal, J. C., Alfieri, L. and E., J.: A high-resolution global flood hazard model, Water Resour. Res., 51, 7785–7789, doi:https://doi.org/10.1002/2015WR016954, 2015.

Sene, K.: Flood warning, forecasting and emergency response, Flood Warn. Forecast. Emerg. Response, 1–303, doi:10.1007/978-3-540-77853-0, 2008.

Singh, P., Sinha, V. S. P., Vijhani, A. and Pahuja, N.: Vulnerability assessment of urban road network from urban flood, Int. J. Disaster Risk Reduct., 28(December 2017), 237–250, doi:10.1016/j.ijdrr.2018.03.017, 2018.

Speight, L. J., Hall, J. W. and Kilsby, C. G.: A multi-scale framework for flood risk analysis at spatially distributed locations, J. Flood Risk Manag., 10(1), 124–137, doi:10.1111/jfr3.12175, 2017.

Sun, W. and Yuan, Y.-X.: Optimization theory and methods: nonlinear programming, Springer Science & Business Media., 2006.

UNISDR: Global Assessment Report on Disaster Risk Reduction. Revealing Risk, Redefining Development, 2011.

Vandebogert, K.: Method of quadratic interpolation, , 1–22, 2017.

Ward, P. J., Jongman, B., Weiland, F. S., Bouwman, A., Van Beek, R., Bierkens, M. F. P., Ligtvoet, W. and Winsemius, H. C.: Assessing flood risk at the global scale: Model setup, results, and sensitivity, Environ. Res. Lett., 8(4), doi:10.1088/1748-9326/8/4/044019, 2013.

Ward, P. J., Jongman, B., Aerts, J. C. J. H., Bates, P. D., Botzen, W. J. W., DIaz Loaiza, A., Hallegatte, S., Kind, J. M., Kwadijk, J., Scussolini, P. and Winsemius, H. C.: A global framework for future costs and benefits of river-flood protection in urban areas, Nat. Clim. Chang., 7(9), 642–646, doi:10.1038/nclimate3350, 2017.

Wei, S., Yuan, J., Qiu, Y., Luan, X., Han, S., Zhou, W. and Xu, C.: Exploring the potential of open big data from ticketing websites to characterize travel patterns within the Chinese high-speed rail system, PLoS One, 12(6), 1–13, doi:10.1371/journal.pone.0178023, 2017.

Winsemius, H. C., Van Beek, L. P. H., Jongman, B., Ward, P. J. and Bouwman, A.: A framework for global river flood risk assessments, Hydrol. Earth Syst. Sci., 17(5), 1871–1892, doi:10.5194/hess-17-1871-2013, 2013.

Winsemius, H. C., Aerts, J. C. J. H., Van Beek, L. P. H., Bierkens, M. F. P., Bouwman, A., Jongman, B., Kwadijk, J. C. J., Ligtvoet, W., Lucas, P. L., Van Vuuren, D. P. and Ward, P. J.: Global drivers of future river flood risk, Nat. Clim. Chang., 6(4), 381–385, doi:10.1038/nclimate2893, 2016.

Wu, Q.: Risk analysis of seismic hazard correlation between nuclear power plants, in Risk Analysis Based on Data and Crisis Response Beyond Knowledge, pp. 550–556, CRC Press., 2019.

Yang, D., Pan, K. and Wang, S.: On service network improvement for shipping lines under the one belt one road initiative of China, Transp. Res. Part E Logist. Transp. Rev., 117, 82–95, doi:https://doi.org/10.1016/j.tre.2017.07.003, 2018.

Zhu, W., Liu, K., Wang, M. and Koks, E. E.: Seismic Risk Assessment of the Railway Network of China's Mainland, Int. J. Disaster Risk Sci., 11(4), 452–465, doi:10.1007/s13753-020-00292-9, 2020.

Appendix
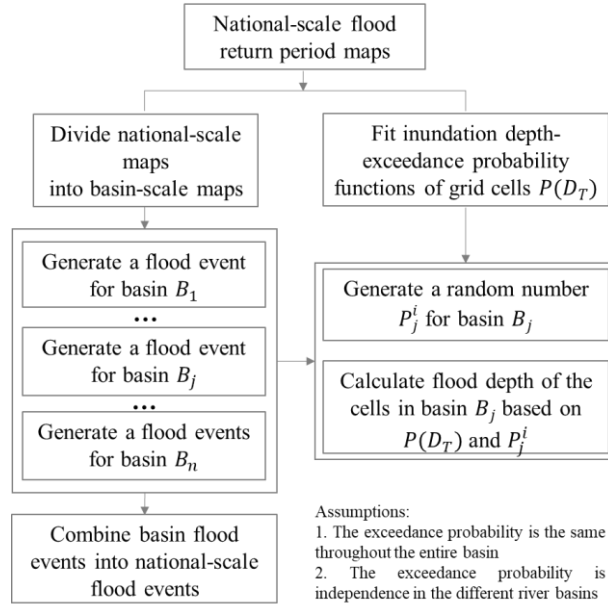
Fig. A1 A flowchart to generate flood event
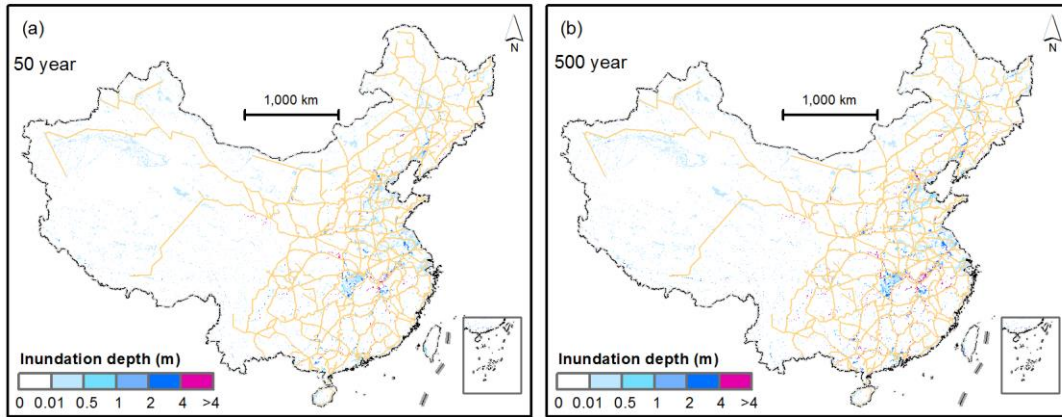
2 *Fig. A2 (a) the 50-year flood, (b) the 500- year flood*
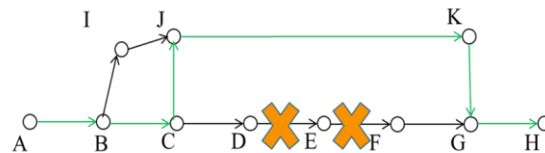
Railway network
Network nodes: $A - K$
Network edges: $AB, ..., KG$
Train trips information:
Trip1:$A \rightarrow B \rightarrow C \rightarrow D \rightarrow E \rightarrow F \rightarrow G \rightarrow H$ (passed and stopped stations)
DE and EF are disrupted by the flood event.

Two routes can complete the detour:
A-B-I-J-K-G-H
A-B-C-J-K-G-H
Based on the 'Pass the most original stations', the green routes have
Been chose for detour.

5 *Fig. A3 An example for detour*
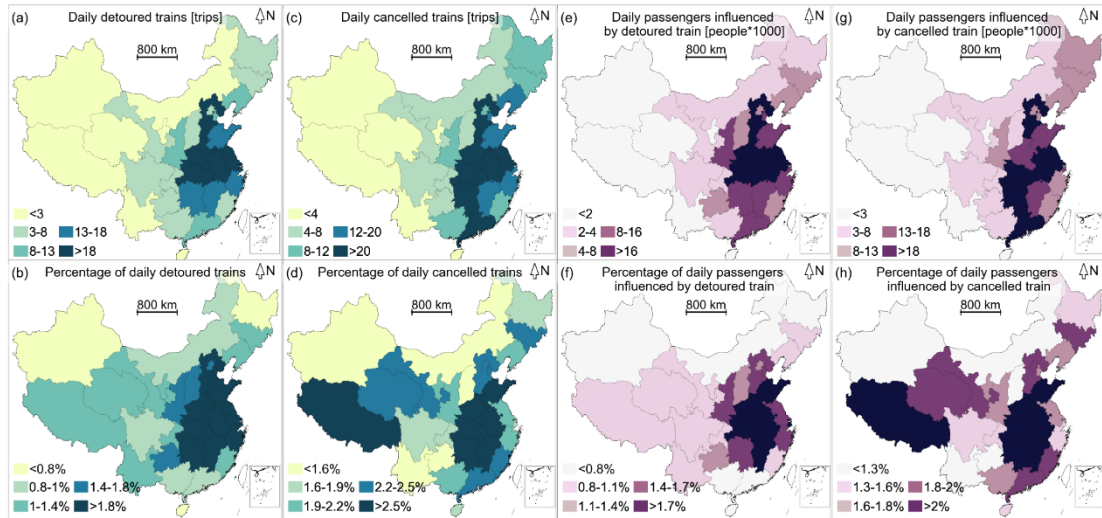
2 *Fig. A4 Performance loss of the railway system per province. (a) presents the daily*

3 *detoured trains in absolute terms; (b) presents the daily detoured trains relative to the*

4 *number of the province's daily trains; (c) presents the daily cancelled trains in absolute*

5 *terms; (d) presents the daily cancelled trains relative to the number of the province's daily*

6 *trains; (e) presents the daily passengers influenced by detoured train in absolute terms;*

7 *(f) presents the daily passengers influenced by detoured train relative to the number of*

8 *the province's daily trains; (g) presents the daily passengers influenced by cancelled train*

9 *in absolute terms; (h) presents the daily passengers influenced by cancelled train relative*

10 *to the number of the province's daily trains.*

2   *Fig. A5 Chinese provinces distribution map. The China Provincial Map layer comes from*

3   *the Data Center for Resources and Environmental Sciences, Chinese Academy of*

4   *Sciences, which is accessible from the Resource and Environment Data Cloud Platform*

5   *(http://www.resdc.cn/, last access: 19 May 2020).*
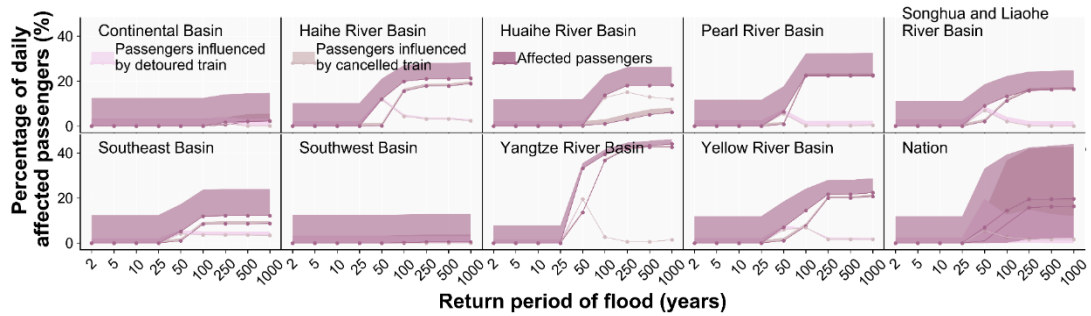
8   *Fig. A6 system-vulnerability curves of passenger's metrics*
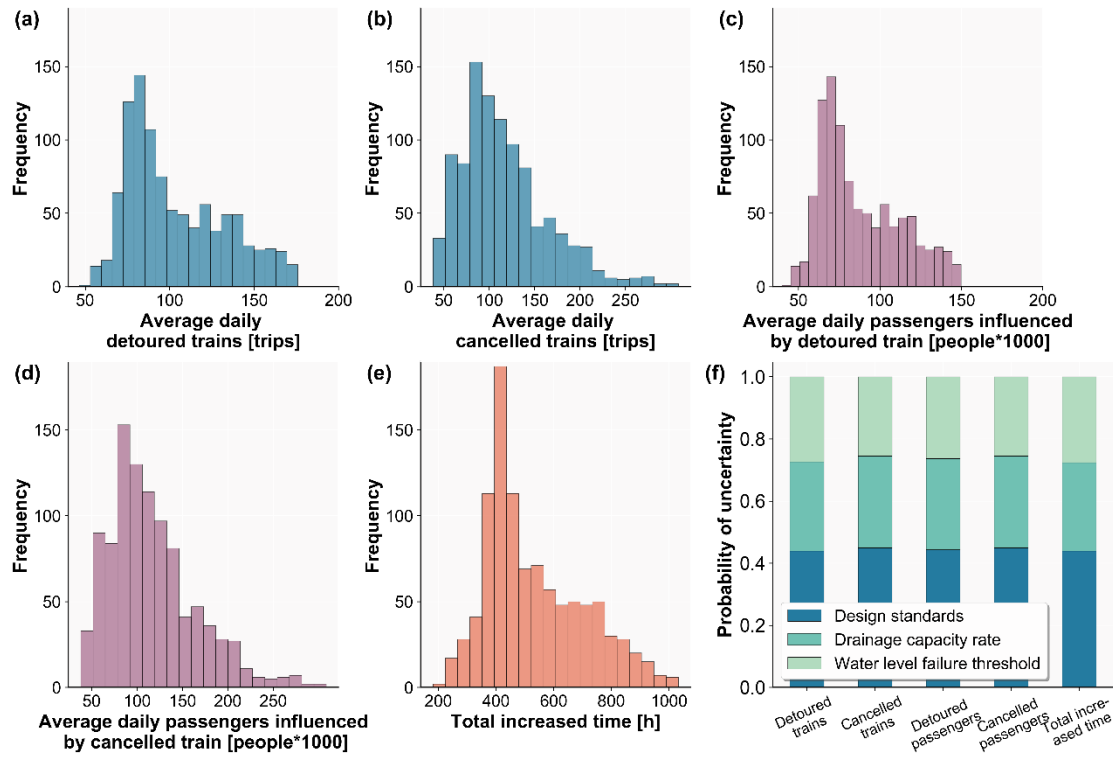
2 *Fig. A7 Results of the uncertainty and sensitivity analyses for the performance metrics.*

3 *(a) average daily detoured trains; (b) average daily cancelled trains; (c) average daily*

4 *passengers influenced by detoured train; (d) average daily passengers influenced by*

5 *cancelled train; (e) total increased time; (f) the sensitivity results.*

1   Table A1 List of data

List of data	
Data	Sources
GLOFRIS global fluvial flood hazard	Ward et al., 2013; Winsemius et al., 2013 (https://datacatalog.worldbank.org/search/dataset/0038584)
River basin map	http://www.resdc.cn/
Geographic railway system	OpenStreetMap (OSM) (https://www.openstreetmap.org/)
Train timetable data	Chinese Railway Service Website (https://www.12306.cn/index/)

3   Table A2 List of variables

List of variables	
Variable	Description
T	Return period of T- year
D_T	The flood depth with return period of T- year
$g_{x,y}$	A grid cell with longitude x and latitude y
$D_{T_{x,y}}$	The flood depth of a flood event of grid cell $g_{x,y}$ with return period of T- year
$P(D_T)$	The annual exceedance probability of flood depth D_T
$Pr(D_T)$	A quadratic, continuously differentiable function of $P(D_T)$
$Pr_{x,y}(D_T)$	A set of continuous inundation depth-exceedance probability functions for $g_{x,y}$
a, b, c	Constant parameters in function $Pr_{x,y}(D_T)$
B_j	River basin j
E_j^i	Flood event i in river basin B_j
P_j^i	A random number between 0 and 1 for flood event E_j^i in basin B_j
Wd	The failure threshold of the railway service after drainage, default value is 0.2
$WL_{x,y}$	The water level after drainage of grid cell $g_{x,y}$
$Wld_{x,y}$	The water level of the flood depth under design standard of grid cell $g_{x,y}$
Dc	The drainage capacity rate of Chinese railway system, default value is 0.8
$Z(xy)$	The failure condition of grid cell $g_{x,y}$
l_{ij}	Rail segment between station i and station j
Fc_{ij}	Failure condition of component l_{ij}
FC_{ij}^e	The failure condition of railway segment l_{ij} under flood event e
AF_{ij}	The annual failure probability of rail segment l_{ij}
E	The N-year flood events catalogue
N_S	The original number of trains in the system
N_e^s	The number of running trains in the system after a flood event
N_e^{tol}	The number of daily affected trains under flood event e
N_e^c	The number of daily cancelled trains under flood event e
N_e^d	The number of daily detoured trains under flood event e

CA_i	The capacity of the ith train
P_e^{tol}	The number of affected passengers
P_e^c	The number of daily passengers influenced by cancelled train under flood event e
P_e^d	The number of daily passengers influenced by detoured train under flood event e
T_i	The original travelling time of the ith train.
T_i^e	The running time of the ith train under flood event e
T_e^{tol}	The total increased time for detoured trains under flood event e
T_e^{ave}	The average increased time under flood event e
AR_s	The expected daily flood risk level to the railway system
V_e	Performance loss metric, including N_e^d, N_e^c, N_e^{tol}, P_e^d, P_e^c, P_e^{tol}, T_e^{tol}, and T_e^{ave}

2 Table A3 List of all assumptions taken in this study and their range in the sensitivity analysis

List of all assumptions taken in this study and their range in the sensitivity analysis		
Varying parameter	Default values	Range
water level failure threshold	0.2m	[0.1m, 0.5m]
drainage capacity rate	0.8	[0.7, 0.9]
design standards	100	[50, 100]